UNIVERSITI MALAYSIA PAHANG

ORIGINAL ARTICLE

Improving Images in Turbid Water through Enhanced Color Correction and Particle Swarm-intelligence Fusion (CCPF)

Syafiq Qhushairy Syamsul Amri[1], Ahmad Shahrizan Abdul Ghani[1,*], Mohd Aiman Syahmi Kamarul Baharin[1], Mohd Yazid Abu[1] and Nagata Fusaomi[2]

[1] Faculty of Manufacturing and Mechatronic Engineering Technology, Universiti Malaysia Pahang, 26600 Pahang, Malaysia.
[2] Sanyo-Onoda City University, Daigakudori, Sanyoonoda, Yamaguchi 756-0884, Japan.

ABSTRACT – When light travels through a water medium, selective attenuation and scattering have a profound impact on the underwater image. These limitations reduce image quality and impede the ability to perform visual tasks. The suggested integrated color correction with intelligence fusion of particle swarm technique (CCPF) is designed with four phases. The first phase presents a novel way to make improvement on underwater color cast. Limit the improvement to only red color channel. In the second phase, an image is then neutralized from the original image by brightness reconstruction technique resulting in enhancing the image contrast. Next, the mean adjustment based on particle swarm intelligence is implemented to improve the image detail. With the swarm intelligence method, the mean values of inferior color channels are shifted to be close to the mean value of a good color channel. Lastly, a fusion between the brightness reconstructed histogram and modified mean particle swarm intelligence histogram is applied to balance the image color. Analysis of underwater images taken in different depths shows that the proposed CCPF method improves the quality of the output image in terms of neutralizing effectiveness and details accuracy, consequently, significantly outperforming the other state-of-the-art methods. The proposed CCPF approach produces highest average entropy value of 7.823 and average UIQM value of 6.287.

INTRODUCTION

An underwater vision in underwater marine, ocean archaeology, ocean biology, ocean research, and ocean security has played increasingly crucial roles. Underwater vision is more complex to use than vision in the open air because raw underwater images have distorted colors and poor image quality [1]. Researchers face many obstacles when exploring insights from marine applications through the detailed study of underwater images. Remotely operated underwater vehicles, underwater archaeology, underwater cable detection, and marine biology research exploration are some of the marine applications. A deteriorated image will have issues with visibility, low contrast, color aberrations, blurriness, and uneven lighting, among other issues [2].

Additionally, different wavelengths of light are absorbed in different ways. Underwater images frequently appear bluish green. To phrase it another way, the level of environmental complexity considerably affects the quality of images underwater. As a result, technologies for underwater image enhancement are crucial for enhancing underwater image quality [3]. Image restoration can be accomplished through the utilization of conventional color correction methods and deep learning-based approaches. In both of these techniques, a distorted image is commonly converted into the CIELAB color space, thereby dividing it into separate chromatic and lightness components [4]. The chromatic component undergoes color correction, while the lightness component is enhanced to generate a dust-free image that closely matches the original. However, conventional image-dedusting techniques overlook the relationship between the depth of scene distortion and the depth of the dust-free image scene, focusing solely on image contrast [4]. Consequently, this approach often results in low color saturation and some remnants of dust in the final output image.

The restoration of hazy, rainy, underwater, and dusty images has been accomplished using a convolutional neural network (CNN) based deep learning method. Leveraging its self-learning capabilities, this deep learning approach requires training the network on a large dataset to generate high-quality restoration results. However, since most networks are trained using synthetic image datasets, certain output images may exhibit insignificant improvements, as the underlying problems are still present in the restored images [4]. In contrast, the proposed CCPF technique utilizes an enhanced color correction method to improve the overall color and contrast of the image, while a modified restoration approach tackles challenges related to image details, brightness reconstruction, and image naturalness. The following contributions have been made:

1. The improved color correction technique involves restoring the red channel, specifically designed for underwater images with different color casts

2. Image neutralizing from the original images is designed by conducting an enhanced brightness reconstruction.
3. Modified mean particle swarm-intelligence-based is implemented to increase the image naturalness.
4. Histogram fusion between the brightness reconstruction and modified mean particle swarm-intelligence-based is conducted to balance the image color.

RELATED WORK

The main reason of suffering underwater images is related to light absorption in water medium and light scattering affects. At the moment, the well-known underwater optical imaging model assumed the camera's light information can be described as a combined linear superposition of direct light I_d, forward scattered light I_f, backward scattered light I_b, and total irradiance, I_T as shown in Equation (1) [5]. I_d is the information about the target contained in the reflected light to the camera. It comes when parts of the reflected light is transmitted at a narrow-angle, resulting in producing a fuzzy image. I_b refers to the spread out medium of ambient light before it got to the camera lens, resulting in contrast reduction of image. The underwater image formulation model can be written as:

$$I_T = I_d + I_f + I_b \tag{1}$$

$$I_\lambda(x) = J_\lambda(X)t_\lambda(x) + \left(J_\lambda(X)t_\lambda(x)\right) * g(x) + B_\lambda\left(1 - t_\lambda(x)\right), \lambda \in \{r, g, b\} \tag{2}$$

Where x is the image pixel's location in space. $J_y(x)$ is the unclouded image with no blurring. $g(x)$ refers to the point distribution function (representing light diffusion results from forward scattering), and B_λ refers to the incident light on the water. $t_\lambda(x)$ is a function of exponential attenuation, that characterises the radiation from the scene that is captured by camera without scattering or absorption and given as Equation (3):

$$t_\lambda(x) = e^{-c_\lambda d(x)} = e^{-(a_\lambda + b_\lambda)d(x)} \tag{3}$$

Where c_λ describes the medium light extinction coefficient with wavelength of λ, $c_\lambda = a_\lambda + b_\lambda$, a_λ is absorption coefficient, while b_λ presents as scattering coefficient. $d(x)$ is distance between the scene point and the camera. b_λ denotes the global water light. $t_\lambda(x)$ decays exponentially with the increasing of d. With regards to Figure 1, it is assumed, that the distance between the scene and the camera is rather short. Thus, the blurry effect that is brought on by forward scattering is ignored. Therefore, Equation (2) can be simplified as follows:

$$I_\lambda(x) = J_\lambda(X)t_\lambda(x) + B_\lambda(X)(1 - t_\lambda(x)) \tag{4}$$
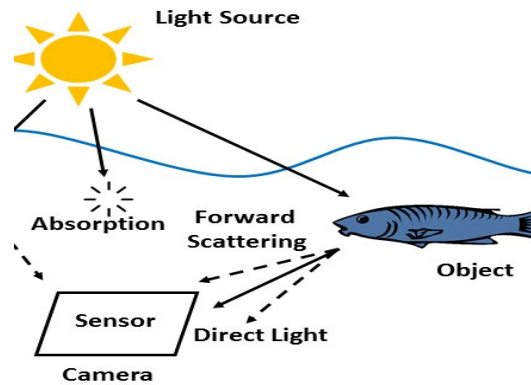
Figure 1. Schematic of underwater image model

Alternatively, Ke et al. [6] described an innovative approach for recovering underwater images through hue matching with the basis of adaptive dark channel prior. Combination of maximum filtering with Gaussian low-pass filtering resulting in accurate prediction of the local water light. For that purpose, they coupled the linear connection between degraded images of dark channel and the attenuation coefficient of clear image.

On the other hand, Zhang et al. [7] suggested a technique for improving underwater images using color correction and adaptive contrast enhancement by conducting tests on a massive real-world database of common underwater images. The algorithm improved the image visibility for both haze and low-level light. However, the algorithm over-enhances regions in underwater images obtained through artificial light. On other report, Zhang et al. [8] introduced a color correction with Bi-interval contrast enhancement technique to produce high-quality natural and underwater landscape images. However, the proposed technique will not be able to generate satisfactory results if high level of noise presents.

Liang et al. [9] introduced a comprehensive approach for enhancing images, which involved utilizing an attenuation map-guided technique for image color correction and a detail-preserving dehazing technique to recover lost details while mitigating the impact of haze. In a similar vein, Wang et al. [10] developed a linear model that takes into account complex

lighting conditions and employed a hierarchical association rule classifier for image color correction. They also utilized axiomatic fuzzy sets to handle complex illumination and implemented a finite-dimensional model for color constancy to improve the image's color. However, although these algorithms succeeded in enhancing the image's brightness, the contrast remains relatively low.

Mohd Azmi et al. [11] presented an enhancement method for deep underwater images that combines color cast removal and optimization algorithms. The method involves two main steps: first, correcting the red color channel based on the dominant green and blue color channels, and second, simultaneously stretching the contrast while enhancing the mean pixels. This approach proves effective for deep underwater images with low red color channel values. However, for turbid underwater images, the method may not yield significant improvements, as the visibility does not reach the desired level. On the other hand, Abdul Ghani et al. [12] focused on improving underwater images by modifying the Lab color model, specifically targeting the reduction of blue-green color casts. However, this method is not sufficiently effective for deep underwater images that are heavily affected by blue-green distortions.

Dutta et al. [13] introduced image enhancement techniques that utilize Particle Swarm Optimization (PSO) and fuzzy logic. The resulting images demonstrate enhanced contrast and exhibit higher Peak Signal-to-Noise Ratio (PSNR) compared to other advanced methods. Furthermore, the low values of Absolute Mean Brightness Error (AMBE) and Normalized Mean Square Error (NMSE) indicate the production of significant output images. In contrast, the Structural Similarity Index Measure (SSIM) of the PSO method is higher than that of the fuzzy method, suggesting the superior performance of the PSO-based image enhancement approach.

Lin et al. [14] presented a stereo-vision detection approach for generating autonomous underwater vehicle (AUV) inspection tasks. This approach utilizes the Bandler-Kohout (BK) triangle sub-product of fuzzy relations and extends the image detection method to enhance the obstacle avoidance capability of AUVs. However, it was observed that the BK technique requires significantly more energy and sailing time compared to the PSO-based method. Taking into account the objectives of minimizing time and energy consumption, the stereo-vision detection approach combined with the PSO-based dynamic routing algorithm is preferred for underwater inspection tasks performed by an AUV.

Swarup Ghosh et al. [15] introduced an artificial particle swarm approach within a fuzzy framework to enhance contrast. The proposed method surpasses conventional techniques such as traditional PSO systems in terms of both subjective and objective evaluations. Shanmugavadivu and Balasubramanian [16] proposed a multi-objective histogram equalization technique using PSO to enhance images. However, this approach proved ineffective in improving both contrast and image brightness. Acharya and Kumar [17] presented the Particle Swarm Optimal Texture-Based Histogram Equalization (PSOTHE) method for enhancing MRI brain images, but it fell short in improving contrast and visibility to the desired level.

Yaqiao et al. [18] introduced an efficient 2-D Otsu lung tissue image segmentation technique using an improved Particle Swarm Optimization (PSO) algorithm. In this method, the search scope of the 2-D grey threshold in the 2-D Otsu algorithm is determined by the neighborhood of the diagonal that connects the third and first sections of the 2-D grey histogram. The PSO algorithm adjusts the particle positions in each iteration based on the symmetric organization principle. Consequently, the diagnostic process of image enhancement needs to be reevaluated to minimize the impact of image artifacts, enhance contrast, and reduce information loss.

Kwok et al. [19] introduced a technique utilizing Particle Swarm Optimization (PSO) for simultaneous image color correction and enhancement. The primary objective of this method is to enhance the information in the image while minimizing the impact of lighting color casts. On a similar note, Wan et al. [20] developed a local entropy-weighted histogram correction approach based on PSO. This method enhances the contrast between foreground and background and emphasizes local features. However, due to low contrast and haziness in the images, it becomes challenging to distinguish objects from the background. In a different study, Kamarul Baharin et al. [21] proposed an image smoothing method specifically for phytoplankton. Their approach involves integrating dual image histogram specification and background removal techniques. The method successfully improves the image through an enhancement process aimed at smoothing, where the image background is completely eliminated to facilitate object identification.

METHODOLOGY

color correction and particle swarm-intelligence fusion

The suggested CCPF approach is intended to adjust and improves the object colour in the image dark regions. There are four significant steps involved: i) Image color restoration, ii) brightness reconstruction, iii) Modified mean swarm intelligence, and iv) histogram fusion. Red colour channel of underwater image will be used as a compensated channel in the first phase of the proposed approach as it has intensity value surrounded with zero as shown in Figure 2. Low intensity value results in producing image color cast as the image is dominant by other color channels. Thus, color restoration step is applied. Next, brightness reconstruction is implemented to enhance the look of the image, primarily by removing undesirable colour casts caused by variations in the light's or the water's quality. Depending on the depth, colour is perceived differently and a green-blue tint may be visible at high depths. The great diversity of currently accessible approaches must be taken into consideration. Third phase is modified mean swarm-intelligence to increase images detail. The histogram fusion is then employed as the last stage in color matching. Figure 3 illustrates the proposed CCPF approach.
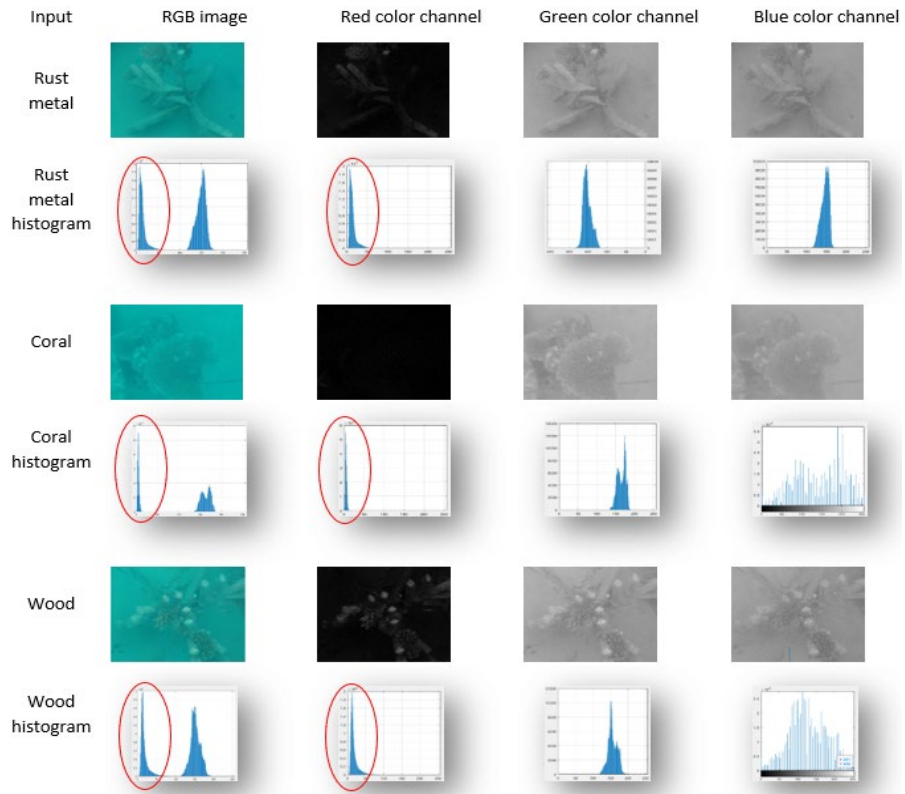
Figure 2. Inferior red color channel has intensity distribution around zero value, middle-centred distribution of green channel pixels and wide-distribution of green channel pixels through the intensity values)
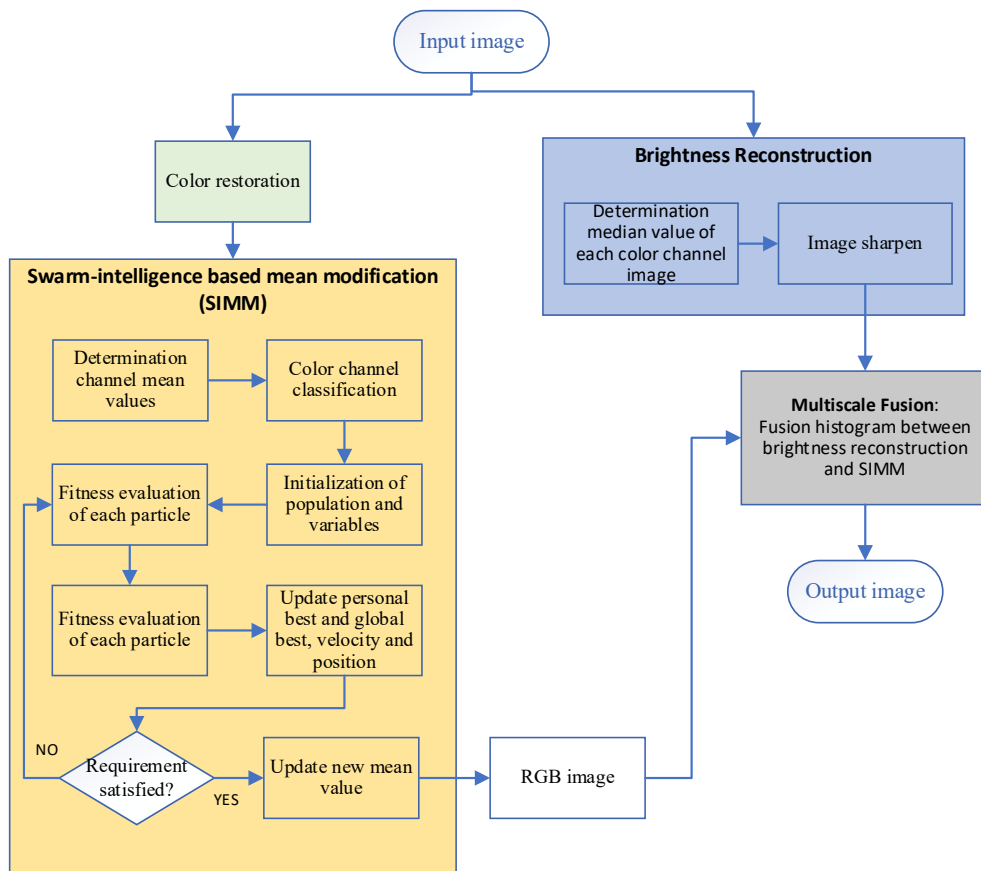

Figure 3. Flowchart of the proposed CCPF method

3.1 Underwater image color restoration

In-depth analysis of heavily damaged underwater sceneries demonstrates that color correction could be more effective to improve image quality [22]. The adjustment which depends solely to intensity color cannot eliminate the color shifting. Grey World and chromatic-modification based techniques are one of the effective ways in removing the color cast. Nevertheless, this method has significant problems with red illumination as it has very low mean value, which results an over-compensation in the areas where red is prevalent.

In addition, the underwater environment in the green channel has been better conserved compared to the red and blue channels due to differences in wavelength. It is crucial to address the stronger signal weakening caused by the red channel. Therefore, we adjust the parameters of the green channel to match the red channel in order to offset the loss in the red channel of the initial image.. Figure 4 demonstrates the effect of color restoration. It is observed that red channel histogram is improved whereas the histogram distribution is shifted to the right near to the histogram centre.
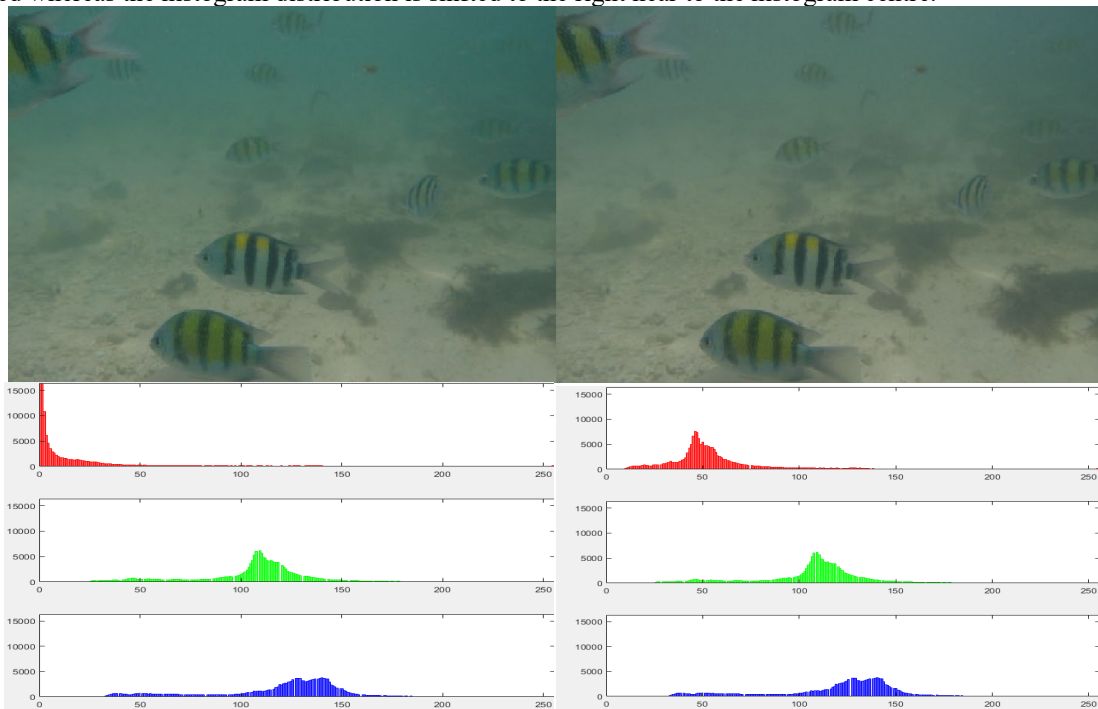
Figure 4. Left is original image and right is recovered image with their respective histograms.

Mathematical expression for the adjusted red channel I_{rc} at each pixel position (x) is given as follow:

$$I_{rc}(x) = I_r(x) + a.(I_g^- - I_r^-).(1 - I_r(x)).I_g(x), \tag{5}$$

where Ir and Ig depict the image's red and green color channels, respectively, with having each channel in the interval of [0, 1], following normalising by the upper limit of their respective dynamic ranges, while I_r^- and I_g^- signify the mean value of Ir and Ig, respectively. In Equation 5, each factor in the second term is a constant parameter that directly comes from one of the above observations. In fact, the experiments have shown that the value of α = 1 is suitable for a variety of lighting conditions and acquisition settings.

As shown in Figure 4, the application of the red channel restoration approach helps eliminate the quantization artefacts caused by domain stretching (the red regions in the different outputs). As the red channel has increases it domination, the reddish color of high intensity areas has been properly addressed.

3.2 Modified mean based on swarm-intelligence (MMSI)

Kennedy and Eberhart [23] introduced a population-based stochastic optimization method known as the PSO approach. This approach utilizes a swarm of particles (agents) to systematically explore the search space and achieve the desired outcome. Each particle retains information about its fitness (ideal value) and the corresponding coordinates in the solution space. These coordinates are referred to as the particle's "personal best" (pbest). Additionally, the PSO algorithm keeps track of the best value achieved by any particle in close proximity, known as the "global best" (gbest). By considering factors such as its current position, velocity, the distance between its current position and its pbest, and the distance between its current position and the gbest, each particle attempts to adjust its location. The particle's velocity is updated according to Equation (6) whenever necessary.

$$P_{out} = 255(\frac{P_{in}}{255})^{\gamma} \tag{6}$$

P_{in} represents the input value of pixel intensity, and P_{out} represents the value output from the pixel. The application determines the value of the constant denoted by γ.

According to the histogram example in Figure 4, each histogram is still in condition of either dark or light. Consequences, the mean value for each RGB space needs to be updated. As required, each color channel needs to be improved by focusing on contrast, object detail, and the inherent color balance of the object. In order to put the CCPF strategy into action, the image will be first split into its individual red, green, and blue color channels in particle swarm intelligence adjustment to get better results. Average value will be obtained for each color channel.

A major contribution of γ to the overall improvement of the image's detail is by selecting a suitable parameter value. The image will become darker if γ is more than 1 and brighter if γ is less than 1. Swarm-intelligence technique is used to calculate automatically the value γ of during this proposed stage.

The PSO technique is employed to bring the average values of less preferred color information closer to the average value of a more desirable color space. PSO was chosen because of its high level of robustness and its ability to converge on the value that optimizes the problem swiftly. This method was implemented by Mohd Azmi et al. [24] to enhance images quality. In this proposed technique of CCPF, the mean value from RBG color channel is used to produces a new significant mean value.
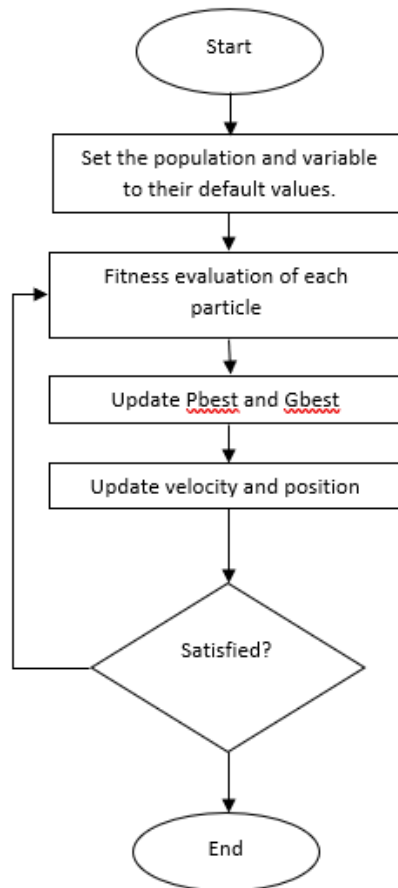
Figure 5. Flowchart of the swarm-intelligence PSO algorithm

Table 1. PSO algorithm parameters implemented in CCPF method

Parameter	Value
Particles Number	30
T_{max}, maximum iteration	60
W_{max}, Weight of maximum inertia	0.9
W_{min}, Weight of minimum inertia	0.4
c1 is cognitive component	2
c2 is social component	2

Following the completion of the initialization stage, the formulation of objective function (*Obj.func*) of swarm-intelligence in the proposed CCPF involves bringing the mean value of dark area color channels as close as possible to the mean value of middle area color channels, as demonstrated by the Equation (7).

$$Obj.func.= [mean\ (Pmax) - mean\ (Pmid)]2 + [mean\ (Pmax) - mean\ (Pmin)]^2 \qquad (7)$$

where $Pmin$, $Pmid$, and $Pmax$ denote the minimum, middle, and maximum mean value of color channels, respectively. $pbest$ refers to the optimal solution discovered by each particle, whereas $gbest$ refers to the optimal personal best. Every time an iteration is performed, both the $pbest$ and the $gbest$ will update a new value. The equation depicting the process of updating the velocities of each particle shows that this process is based on the Equation (8).

$$v_i^t = \omega^t v_i^t + c_1 rand(P_{best} - x_i^t) + c_2 rand(g_{best} - x_i^t) \qquad (8)$$

where the particle position i at iteration t, denoted by x_i^t, and its velocity, denoted by v_i^t, are respectively considered. $rand$ refers to numbers between 0 and 1 that are selected at random. c_1 and c_2 stand for the cognitive and social coefficients, whereas ω^t stands for the weight inertia at iteration t. In the given algorithm, linear dynamic weight inertia is utilized and calculated based on Equation (9).

$$\omega^t = \omega_{max} - \left(\frac{\omega_{max} - \omega_{min}}{t_{max}}\right) \text{x } t \qquad (9)$$

where ω_{max} and ω_{min} represent the highest and lowest possible values of weight inertia, respectively, t_{max} is the number of iterations will be repeated. The new velocity v_i^t of the particle is applied to the equation for the purpose of updating the particle position and calculated using the following Equation (10):

$$x_i^t = x_i^t + v_i^t \qquad (10)$$

(a)   (b)
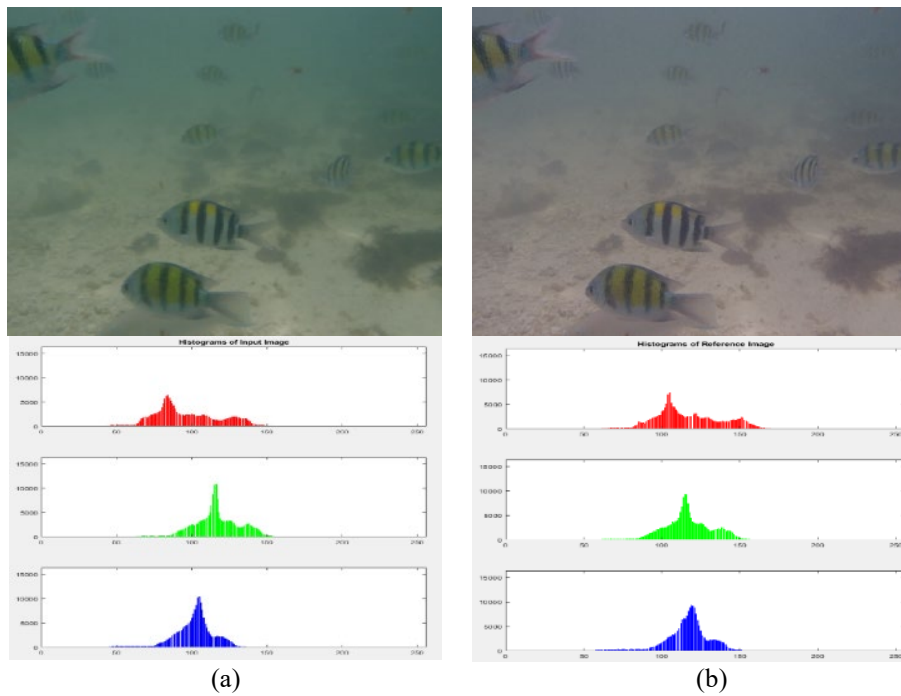
Figure 6. Figures shows red recovered image from (a) previous step and (b) output image after MMSI implementation

3.2 Brightness reconstruction

In the meantime, brightness needs to be developed to get the correct object's color. Reconstructing an image's brightness serves the purpose of removing any dark areas in an image prior to fusing it with other procedures. The proposed approach achieves brightness reconstruction with the following process in order to improve the object color:
Step 1: Image inversion.
Step 2: Murk reduction process through haze removal method.
Step 3: Image re-inversion.
Based on the following equation, the input image is inverted:

$$R_C(X) = 255 - I_C(X) \qquad (11)$$

The term $R_C(x)$ designates Red, Green, and Blue as the output colour channels, respectively. The color channel input intensity for the low-light image is $I_C(X)$. $R_C(X)$ and the inverted image R both have the same intensity. However, the haze removal technique is implemented as follows:

$$R(x) = J(x)t(x) + A(1 - t(x)) \qquad (12)$$

where A represents the ambient atmospheric light. $R(x)$ denotes as the captured intensity pixel x. $J(x)$ represents the intensity OF original object or scene. $t(x)$ describes the proportion of the scene's or object's emitted light that reaches the camera. A crucial aspect of all haze removal techniques is the estimation of A and $t(x)$ from the captured image intensity $I(x)$ in order to recover $J(x)$ from $I(x)$. When the atmosphere is homogenous, the expression for $t(x)$ is:

$$t(x) = e - \beta d(x) \qquad (13)$$

where β is the scattering coefficient while $d(x)$ is the scene depth of pixel x. t(x) is given by d(x) represents the distance between the object and the camera when the β is constant. t(x) is calculated using the following Equation (14):

$$t(x) = 1 - \omega \min_{c \in \{r,g,b\}} \left(\min_{y \in \Omega(x)} \left(\frac{R^c(y)}{A^c} \right) \right) \qquad (14)$$

Where ω is 0.8 according to the default value Kamil et al. [22]. $\Omega(x)$ is a local block centred on x with a block size of 9. In this work, this algorithm is used to estimate $t(x)$. To estimate the global atmosphere light, A, 100 pixels with the highest minimum intensities in all color (RGB) channels are chosen. Then, among the pixels, the one pixel with the highest sum of RGB values is selected. Next, the pixel with the largest RGB total is picked to represent the letter A. As a result, $J(x)$ is obtained as follow:

$$J(x) = \frac{R(x) - A}{t(x)} + A \qquad (15)$$

It has been determined that the direct use of equation (15) may result in under-enhancement for low-lighting regions. To optimise the calculation of $t(x)$, it should be adapted adaptively while keeping its spatial continuity. Thus, the resulting image becomes visibly smoother. $P(x)$ is set as follow:

$$P(x) = \begin{cases} 2t(x), & 0 < t(x) < 0.5 \\ 1, & 0.5 < t(x) < 1 \end{cases} \qquad (16)$$

When $t(x)$ is smaller than 0.5, indicating that the corresponding pixel requires enhancement, provide a small value to $P(x)$ make $P(x)t(x)$ even smaller, thereby increasing the RGB intensities of this pixel. When $t(x)$ is greater than 0.5, we refrain from excessively raising the corresponding pixel intensity. Thus,

$$J(x) = \frac{R(x) - A}{P(X)t(x)} + A \qquad (17)$$

The outcome of the improvement after the brightness and precision adjustment was applied may be seen in the following figure. As a result of the low illumination level, the original image with inferior lighting (Figure 7 (a)) only displays a very limited amount of scene information. Figure 7d illustrates the improved outcome, in which the image's visibility, brightness, and color have greatly improved. Additionally, brightness is significantly improved, particularly in the backdrop and the darker sections. The histogram of the image that was output may be seen in Figure 8.

(a)   (b)

(c)   (d)

Figure 7. Comparison of the resultant images from previous steps (a) The original image with poor illumination. (b) Inverted image. (c) Dehazed image. (d) Re-inverted image.
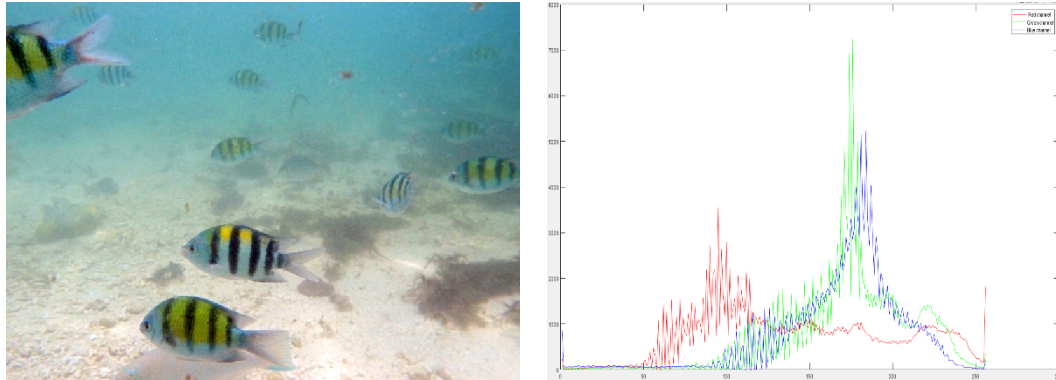

Figure 8. Resultant RGB image and its histogram after dehazing and inversion processes.

This comparison as depicted in Figure 9 is to demonstrate the brightness reconstruction process, which leads to enhanced color distribution in the image. This process is also capable of addressing white balance issues such as grey world, white patch, and chromatic adaptation. White balance helps eliminate undesired color tints caused by varying illumination conditions or medium attenuation properties. The perception of color alters as one goes deeper into the water. Furthermore, the distance between the observer and the scene impacts both attenuation and color degradation.

Original Image   *White patch*   *Gray World*   *Chromatic adaptation*   *Brightness Reconstruction*
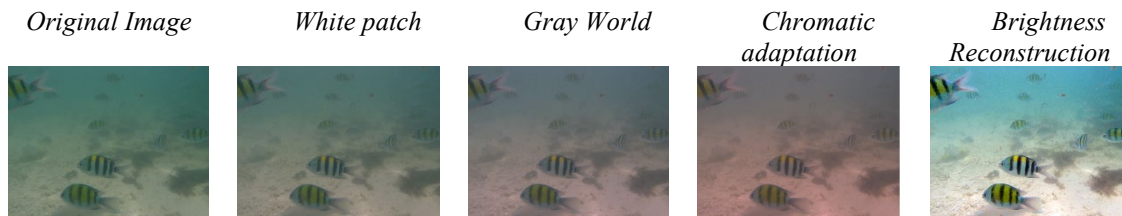
Figure 9. Comparison of the brightness reconstruction as compared with other white balance algorithms.

3.4 Multi-scale fusion

Image compositing, high dynamic range (HDR) imaging and multispectral video images are applications that demonstrate image fusion's usefulness. In this context, we are looking for a simple and efficient method that can improve the scene's visibility in a wide variety underwater image. Figure 10(a) shows the original images before the brightness reconstruction is applied. In Figure 10(b), the produced under- and over-enhanced images are integrated by mean values and implemented with brightness reconstruction and produces image in Figure 10(c). The steps for this process are as follow:

Step 1: Obtain the histogram for both the images, input image (Figure 10(b(i))) and the image that was specified image b(ii) (Figure 10). The calculation of the input image is done based on the following equation:

$$h_{input}(i) = P_i \tag{18}$$
$$h_{specified}(i) = P_i \tag{19}$$

Where i is the number of pixels of intensity level. P is probability density function and h is normalized histogram.

Step 2: Obtain the cumulative distribution function (CDF) for both; input image as well as the specified image. The cumulative distribution function $H(j)$ is defined as the probability that a randomly picked pixel would have one of the

intensity values ranging from 0 to 255 for 8-bit image. This probability is expressed as a percentage. It can be derived by the following formula:

$$CDF = H(j) = \sum_{i=0}^{j} h(i) \quad where\ j = 0,1,\dots\dots,254,255 \qquad (20)$$

Step 3: Determine the transformation T for mapping the old intensity values into the new intensity values. Let k stand for the total number of different intensities that can be achieved (e.g., 256). j represents the previous intensity value, and $T(j)$ represents the new intensity value.

$$T_{input}(j) = floor((k-1) * CDF_j) \qquad (21)$$
$$T_{specified}(j) = floor((k-1) * CDF_j) \qquad (22)$$

Step 4: Mapping the input image's intensity values to new values using the transformed intensity values for both the input image and the selected image.

Fusion process

Histogram mapping is applied in order to increase the image detail. The image intensity values of the output image are remapped by the process of contrast enhancement so that they fall within the full dynamic range of the data type. The histogram is applied with contrast stretching in order to make adjustments to the brightness and contrast of an image. During this step of the procedure, pixel values that are less than or equal to the threshold value are mapped to the black color, whilst pixel values that are equal to or greater than the threshold value are assigned to the white color. The final result is a linear mapping between a selection of pixel values and the whole range of display intensities (dynamic range). Following the fusion process, an example of the output image together with its histogram can be shown in Figure 10. It was observable that the color as well as the image details of the output images had been significantly improved.
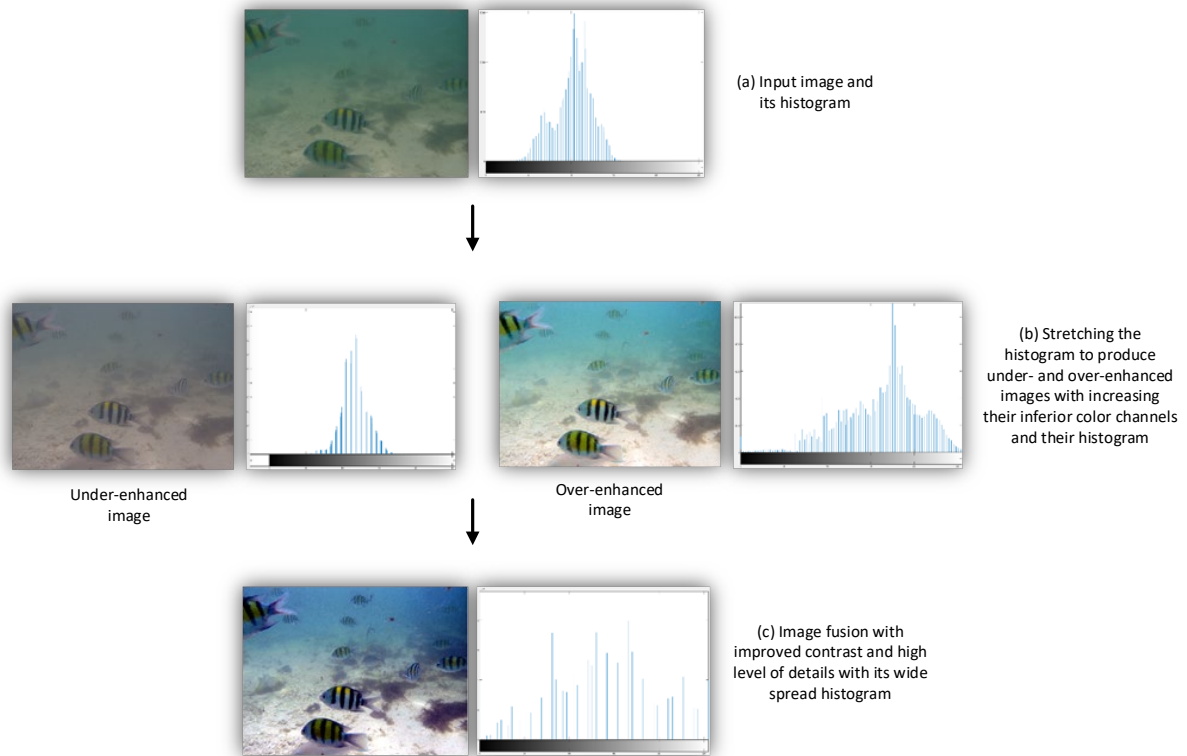
Figure 10. The image shows the output image (c) and its histogram after implementation of histogram fusion.

The effect of brightness reconstruction can be seen clearly in the image during the first stage, where Figure 10(a) demonstrates that the dark parts appear darker, and Figure 10(c) demonstrates that the dark areas appear whiter when compared to Figure 10(a). Figures 10(a) and 10(c) illustrate the histogram of the images before and after the brightness modification is applied.

EXPERIMENTAL RESULTS

This The effectiveness of the proposed CCPF method is proved by comparing it to a number of other state-of-the-art methods within the similar study domain. These are natural-based underwater image (NUCE) [24], Brightness Preserving Dynamic Histogram Equalization (BPDHE) [25], Histogram Equalization (HE) [26], Adaptive Multiscale Retinex (AMSR) [27], Low-Light Image Enhancement (LIME) [28], Low-Light Image Enhancement (ICCV) [29], and Rayleigh CLAHE [30]. These compared approaches are chosen for comparison since they are from the same study domain and are based on histogram and color correction adjustment. For the experiment, around ten sample images are chosen to assess and show the effectiveness and reliability of the suggested CCPF approach in improving the underwater image. These underwater images suffered from low contrast, limited visibility, murky surroundings, and heavily influenced by blue-green sea water.

Evaluations on both a qualitative and quantitative are carried out to verify if the proposed CCPF method is able to improve the object's detail as well as its visibility in underwater images. Quantitative analysis comprises not only the measurement of images attributes but also the use of probabilistic statements related with identification, such as mistake rates. This type of analysis is performed using statistical evaluation. Additionally, the techniques of image analysis are presented together with some parameters including feature extraction and results verification.

4.1 Qualitative evaluation

Figure 11 illustrates the challenging task of identifying objects and the resulting mismatched colors in the original images. Furthermore, the original image exhibits other distortions such as low contrast and color deviations. On the other hand, the outcomes achieved through the CCPF approach are satisfactory, as it successfully enhances the visual aspects of the image. The final image also effectively showcases detailed texture information.
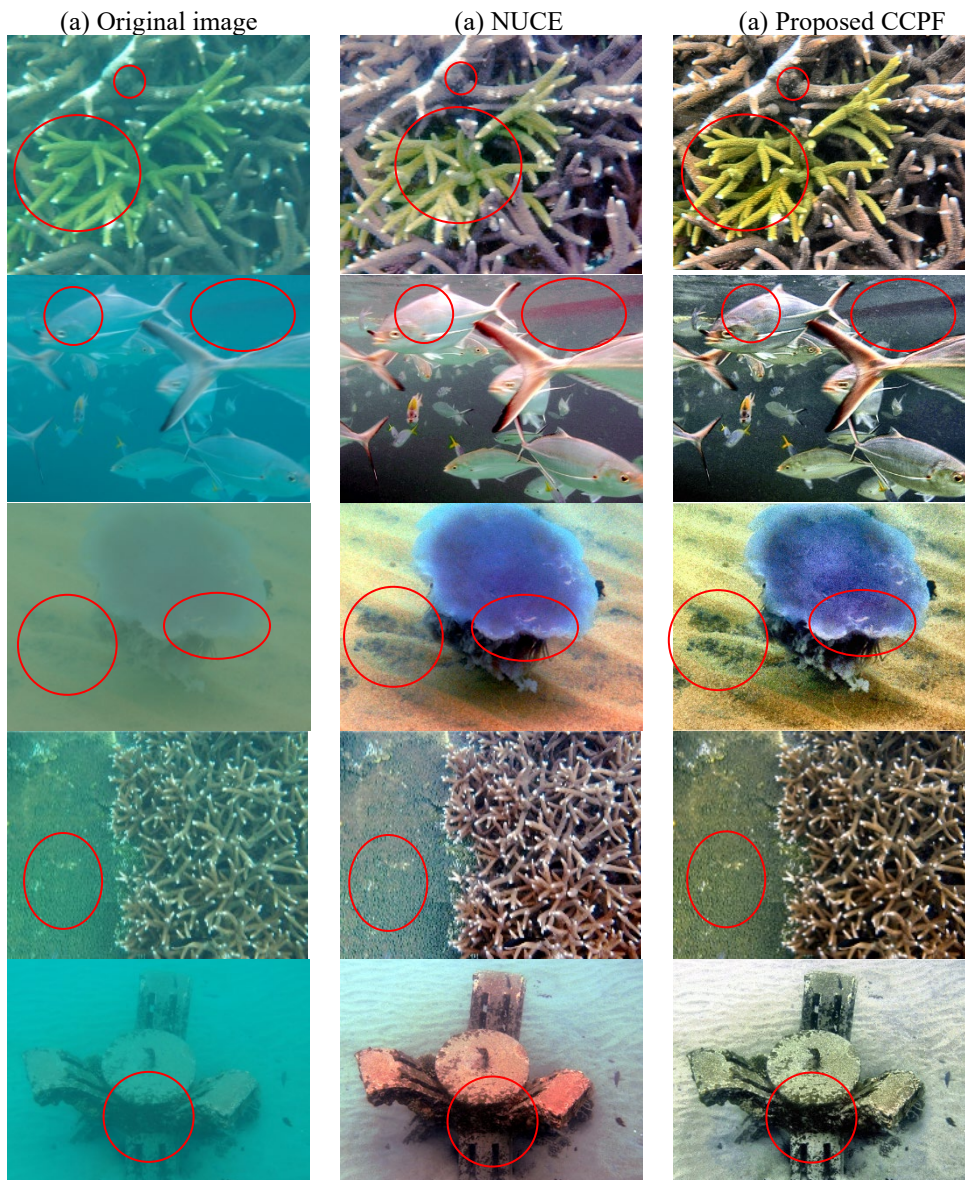
Figure 11. Results of a fish image, (a) Original image; (b) (NUCE) (c) Proposed CCPF method.

Figures 12A and 12B provide a comparison between the proposed CCPF approach and other state-of-the-art methods. When compared to the original images, the output images of the HE method exhibit specific objects with a significantly increased brightness level. The CLAHE-Rayleigh and NUCE methods produce similar results to the proposed CCPF approach, revealing a high level of detail as the objects' structure and features become clear. AMSR, on the other hand, appears to have a darker tone compared to the others. In terms of object structure detail, CLAHE-Rayleigh, HE, AMSR, LIME, and NUCE demonstrate more clarity than the CCPF method. However, the BPDHE method does not improve image details but instead preserves the blueish and greenish tones from the original image in the final result.

In addition, CCPF approaches are effective at bringing out the details in the shadows and smoothing out the overall image. On the other hand, based on the visual evaluation of the CCPF approach, an overall improvement in details and visibility could be seen quite plainly in the images that are produced. The contrast in the image that is generated by CCPF is quite high since the image is very clear, and the subjects can be identified from the environment very well.
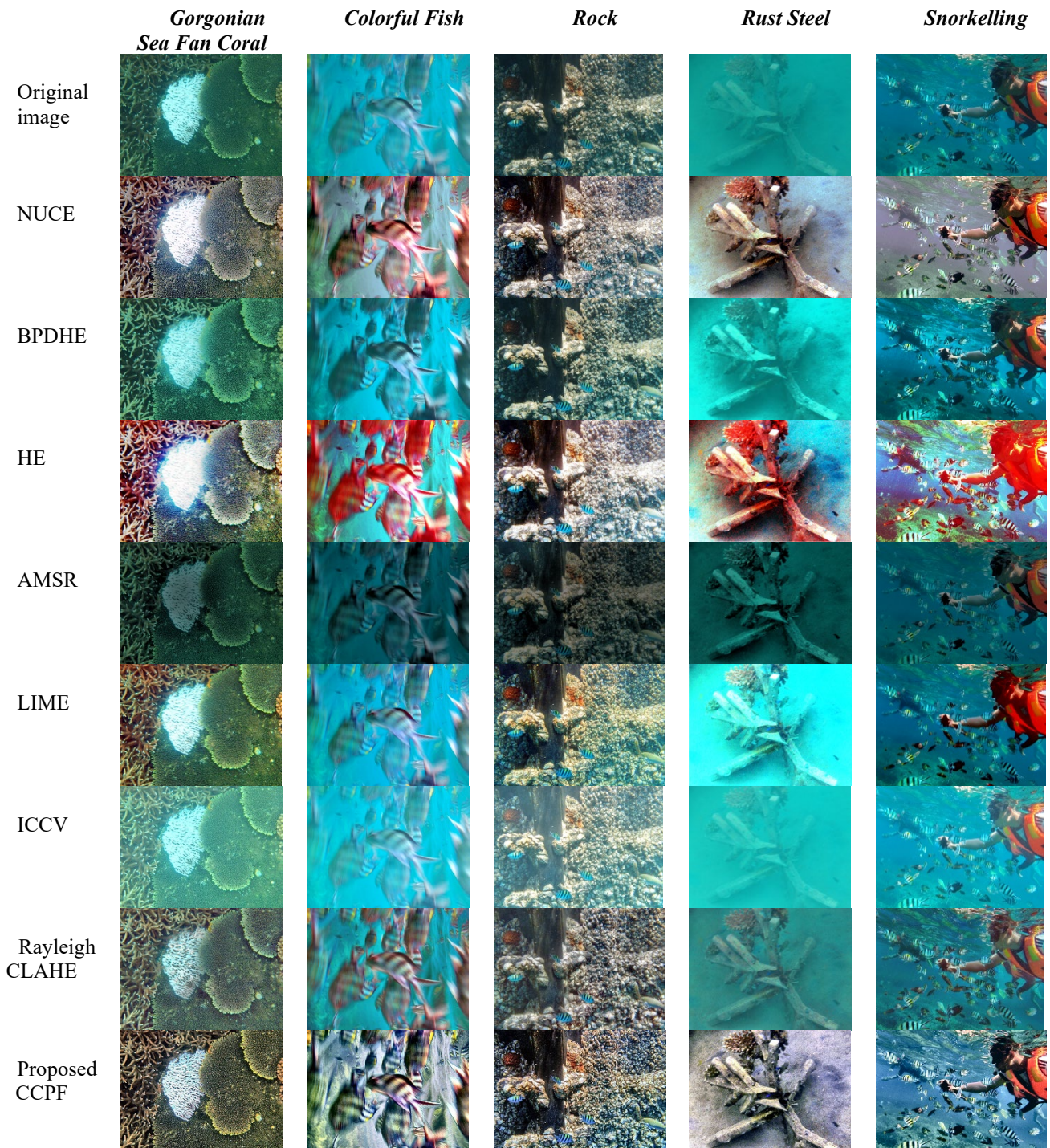
Figure 12A. Comparison between the proposed CCPF method and state-of-the-art methods.
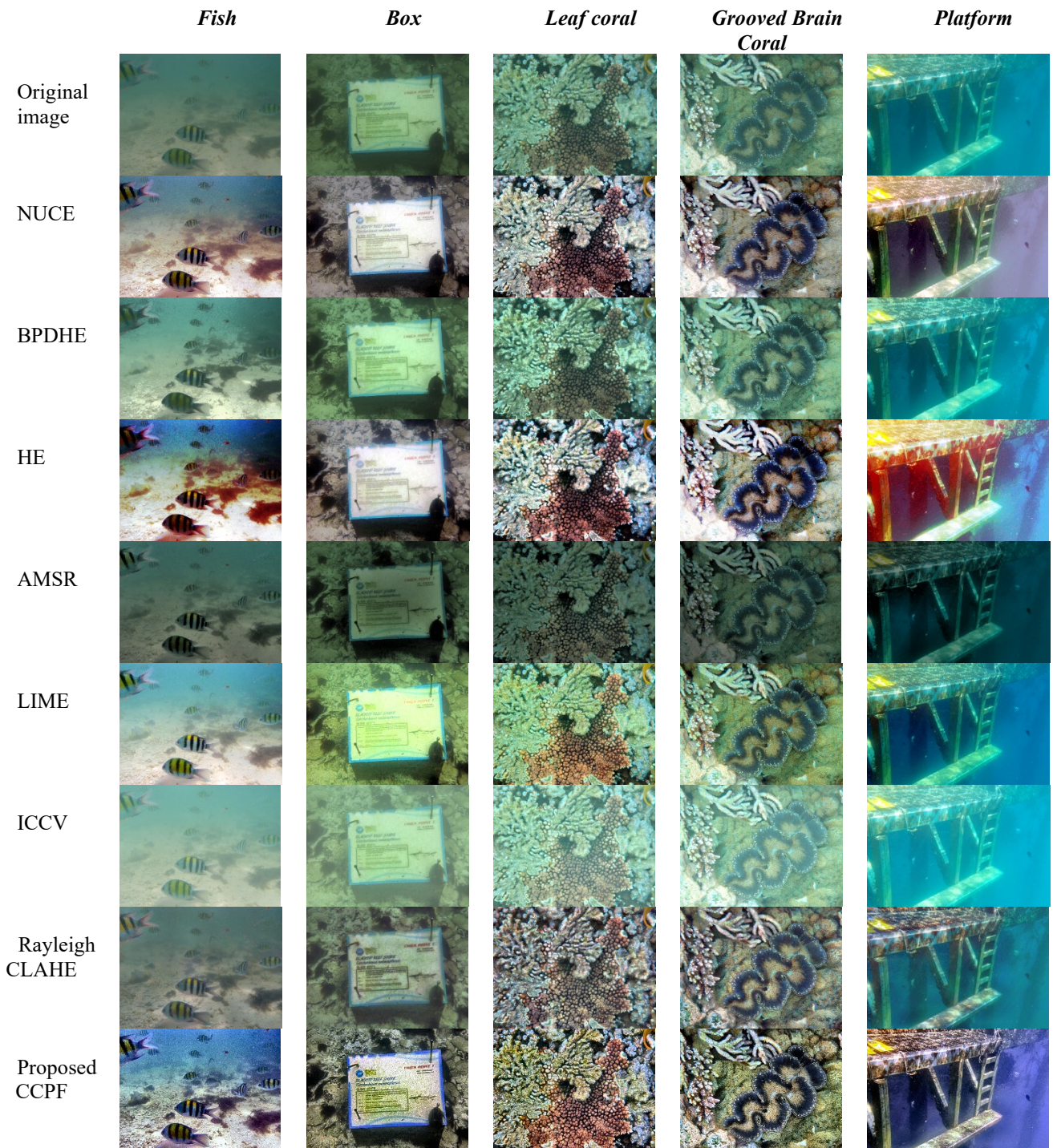
Figure 12B. Comparison between the proposed CCPF method and state-of-the-art methods.

4.2 Quantitative Evaluation

The effectiveness of the proposed CCPF approach is demonstrated through both qualitative and quantitative evaluations. The quantitative evaluation, in particular, supports the qualitative findings. To achieve this objective, several quantitative parameters such as entropy [31], underwater image quality measure (UIQM) [32], underwater color image quality evaluation (UCIQE) [33], mean-squared-error (MSE) [34], peak signal-to-noise ratio (PSNR) [35], perception-based image quality evaluator (PIQE) [36], and naturalness image quality evaluator (NIQE) [37] are utilized as indicators of effectiveness.

Entropy is a statistical measure of unpredictability used to characterise an image's texture. $H(x)$ is defined as follows:

$$H(x) = -\int_{x=1}^{k} p(x) \, log_2 p(x) \qquad (23)$$

where p is the image's PDF at state x (pixel) and k denotes the number of grey levels. Entropy quantifies the quantity of image data or image features. The greater the entropy value, the higher the image quality.

Equation (24) demonstrates the mathematical formulation of UIQM, which is composed of three factors: underwater image sharpness measure (UISM), underwater image colorfulness measure (UICM), and underwater image contrast measure (UICM), underwater image contrast measure (UIConM).

$$UIQM = C_1 * UICM + C_2 * UISM + UIConM \tag{24}$$

UIQM is an evaluation parameter based on the human visual system that measures the quality of underwater images. A higher UIQM number indicates image quality. The UCIQE metric for underwater images is represented by Equation (25).

$$UCIQE = c_1 * \sigma_c + c_2 * con_l + c_3 * \mu_s \tag{25}$$

where σ_c is the chroma standard deviation, con_l is the luminance contrast, and μ_s is the average saturation with weighted coefficients $c_1 = 0.4680$, $c_2 = 0.2745$, and $c_3 = 0.2576$. For high image quality, the UCIQE parameter must be high.

In addition to that, the suggested method utilizes MSE and PSNR as they are commonly used quality assessment metrics in previous studies and widely employed for image evaluation purposes. MSE is employed to measure signal fidelity and compare the level of error or distortion between two signals by generating a statistical score. It is calculated by averaging the squared changes in intensity between the pixels of the distorted and reference images. The equation (26) represents the metric for MSE.

$$MSE = \frac{1}{M \times N}\sum_{M,N}[I_1(m,n) - I_2(m,n)]^2 \tag{26}$$

Where intensity value of the original (reference) and improved images defines as $I_1(m,n)$ and $I_2(m,n)$. M, N represents the size of the image, while m and n represent the x and y coordinates of the image's pixels. The lower the MSE number, the less noise and error. However, MSE is typically expressed as PSNR. Signal-to-noise ratio (PSNR) is the ratio between the highest potential signal and the noise that affects the image representation. The equation (27) for PSNR expressed as:

$$PSNR = 10\,log_{10}\frac{(2^B-1)^2}{\sqrt{MSE}} = 20log_{10}\frac{(2^B-1)}{\sqrt{MSE}} \tag{27}$$

Where $(2^B - 1)$ refers to the image's highest signal strength. r, B = 8 as the unsigned integer 8 image is used. The maximum possible signal becomes 255 or $(2^B - 1)$. The maximum intensity value for an image in unsigned integer 8 format is 255. A high PSNR value suggests great image quality.

Finally, the assessment of image quality incorporates the use of the Naturalness Image Quality Evaluator (NIQE). NIQE calculates a no-reference image quality score, where a lower score indicates higher perceptual quality. It estimates the disparity between the image features based on natural scene statistics (NSS) and the features derived from the image database used to train the model. On the other hand, the Perception-based Image Quality Evaluator (PIQE) calculates a quality score by evaluating both an image and its corresponding distorted version. PIQE derives a no-reference quality score by estimating block-wise distortion.

According to the quantitative findings presented in Table 2, the CCPF approach that has been proposed, provides better detailed information regarding the texture, and it is clearly shows in Figure 13, that the values for all of the measurement analyses are neither too high nor excessively low. As an illustration Figure 13, the values of UIQM and UCIQE are not all that different from one another. The same as the PIQE and NIQE scores. The CCPF method shows the balance color of the object and does not focus specifically on a single measurement as a result of this. This demonstrates that the CCPF technique was successful in enhancing the image detail. This method is in the first best position for entropy and UIQM evaluation.

Table 2. Dataset for the images in Figures 12A and 12B for the quantitative evaluation of the proposed CCPF approach and numerous state-of-the-art methods in terms of entropy, UIQM, UCIQE, MSE, PSNR, PIQE, and NIQE

Image	Methods	Quantitative analysis						
		Entropy ↑	UIQM ↑	UCIQE ↑	MSE ↓	PSNR ↑	PIQE ↓	NIQE ↓
	Input	7.204	3.856	0.528	-	-	42.278	**3.983**
	NUCE	7.653	4.496	0.625	2.490	14.161	44.724	4.067
Image 1	BPDHE	7.491	3.698	0.536	493.98	**21.194**	51.105	4.737
(Gorgonian	HE	5.900	4.255	0.655	4.850	11.271	48.260	4.476
Sea Fan Coral)	AMSR	6.784	**5.180**	**8.801**	9.429	8.386	43.067	4.115
	LIME	7.419	4.617	0.620	**1.108**	17.685	45.322	4.273
	ICCV	7.283	5.129	0.420	9.360	8.418	43.099	4.093
	RCLAHE	7.302	5.112	0.555	1.306	16.971	**40.094**	4.406

	CCPF	**7.661**	4.260	1.411	9.391	8.404	44.210	4.671
Image 2 (Colorful fish)	Input	7.313	-	0.424	-	-	43.679	3.614
	NUCE	7.699	4.318	0.662	5.390	10.815	**21.659**	3.984
	BPDHE	7.548	0.276	0.510	475.717	21.357	38.462	**3.412**
	HE	5.830	5.093	0.700	6.748	9.839	27.353	4.090
	AMSR	6.625	3.886	**17.336**	2.005	5.111	37.625	3.501
	LIME	7.321	0.078	0.497	151.295	**26.333**	33.141	3.531
	ICCV	7.282	3.769	0.545	1.993	5.135	35.942	3.540
	RCLAHE	7.354	2.825	0.562	**1.729**	15.754	26.406	3.684
	CCPF	**7.918**	**5.695**	1.548	1.998	5.125	31.809	6.065
Image 3 (Rock)	Input	7.473	5.056	0.569	-	-	20.285	2.885
	NUCE	**7.868**	5.169	0.621	**1.535**	16.269	25.078	3.109
	BPDHE	7.642	5.006	0.581	370.937	**22.438**	23.264	**2.840**
	HE	5.984	5.390	0.626	3.049	13.289	19.367	3.335
	AMSR	6.807	5.355	17.375	9.542	8.334	18.228	3.141
	LIME	7.813	5.059	0.635	1.545	16.242	20.541	3.384
	ICCV	7.381	5.377	**50.950**	9.468	8.368	19.259	3.125
	RCLAHE	7.578	5.451	0.571	919.954	18.493	**15.783**	3.490
	CCPF	7.835	**16.366**	1.456	9.493	8.357	38.895	5.299
Image 4 (Rust steel)	Input	6.083	0.075	0.295	-	-	27.499	4.650
	NUCE	7.715	4.615	0.631	7.478	9.393	37.202	6.399
	BPDHE	7.021	0.295	0.407	**1.228**	17.239	17.444	**4.383**
	HE	5.674	4.947	0.725	9.035	8.571	28.766	5.508
	AMSR	6.353	4.846	**7.792**	1.479	6.432	13.436	4.846
	LIME	5.991	1.789	0.423	5.489	10.736	13.840	4.549
	ICCV	6.178	3.636	0.267	1.469	6.460	22.665	4.742
	RCLAHE	6.714	1.891	0.380	793.700	**19.134**	**12.532**	4.842
	CCPF	**7.848**	**5.146**	1.286	1.473	6.450	48.136	7.862
Image 5 (Snorkelling)	Input	6.786	1.085	0.547	-	-	34.143	3.322
	NUCE	7.260	4.420	0.626	**4.678**	11.430	**19.490**	**2.761**
	BPDHE	7.026	1.743	0.586	379.416	**22.340**	29.689	3.333
	HE	5.625	5.454	0.682	7.528	9.364	31.860	3.760
	AMSR	6.266	3.887	22.522	9.947	8.154	32.730	3.033
	LIME	6.553	1.463	0.655	617.552	20.224	26.597	3.132
	ICCV	6.973	3.612	41.599	9.891	8.179	27.184	3.550
	RCLAHE	6.783	3.130	0.555	602.079	20.334	20.590	3.470
	CCPF	**7.726**	**6.037**	**60.86**	9.908	8.171	31.239	3.731
Image 6 (Fish)	Input	6.430	0.997	0.413	-	-	20.155	4.140
	NUCE	7.647	3.952	0.632	2.647	13.904	30.545	4.380
	BPDHE	7.260	1.955	0.636	1.612	16.056	22.870	**3.366**
	HE	5.876	3.104	0.507	4.131	11.970	26.002	3.742
	AMSR	6.331	4.596	0.677	1.084	7.781	14.541	3.843
	LIME	7.414	1.929	31.169	4.31	11.788	12.135	3.596
	ICCV	6.508	3.718	0.561	**1.078**	7.806	15.719	4.139
	RCLAHE	6.507	2.586	0.426	217.319	**24.760**	**11.723**	3.579
	CCPF	**7.727**	**5.284**	52.111	9.908	8.171	30.622	3.638
Image 7 (Box)	Input	7.184	2.094	0.461	-	-	23.108	2.757
	NUCE	7.875	4.300	0.579	2.442	14.253	21.924	3.484
	BPDHE	7.542	2.447	0.510	656.199	19.960	23.986	**2.650**
	HE	5.988	3.248	0.591	2.792	13.671	21.097	2.940
	AMSR	6.923	5.500	**6.472**	1.052	7.913	19.042	2.784
	LIME	7.614	3.047	0.560	2.870	13.553	18.239	3.220
	ICCV	6.938	4.237	0.446	**1.045**	7.941	**16.195**	2.747
	RCLAHE	7.112	3.834	0.458	599.039	**20.356**	18.876	2.682
	CCPF	**7.914**	**5.835**	1.937	1.047	7.932	47.104	4.421
Image 8 (Leaf coral)	Input	7.331	4.293	0.481	-	-	22.873	4.830
	NUCE	**7.894**	4.823	0.622	1.544	16.245	21.858	4.830
	BPDHE	7.578	4.525	0.530	218.910	**24.728**	27.819	**4.609**
	HE	5.988	5.030	0.643	1.944	15.243	27.723	4.922
	AMSR	6.868	5.137	**10.478**	1.390	6.702	22.159	4.707

	LIME	7.750	4.593	0.587	**1.091**	17.752	**18.396**	5.019
	ICCV	7.314	5.055	0.515	1.381	6.729	21.222	5.055
	RCLAHE	7.708	**5.560**	0.584	943.06	18.385	21.304	4.994
	CCPF	7.891	4.321	1.732	1.385	6.718	32.340	5.230
Image 9 (Grooved Brain Coral)	Input	7.372	3.785	0.489	-	-	24.765	4.227
	NUCE	7.840	5.008	0.615	973.080	18.249	31.217	4.756
	BPDHE	7.582	3.886	0.510	206.428	**24.983**	26.620	4.250
	HE	5.987	4.916	0.631	1.849	15.461	31.361	4.185
	AMSR	6.747	5.170	13.911	1.543	6.248	23.050	**4.038**
	LIME	7.651	4.532	0.575	247.626	24.193	**24.324**	4.701
	ICCV	7.253	4.594	**13.982**	**1.533**	6.276	24.761	4.259
	RCLAHE	7.542	**5.336**	0.571	921.54	18.486	25.486	4.555
	CCPF	**7.902**	4.859	1.387	1.537	6.263	38.321	5.263
Image 10 (Platform)	Input	6.982	0.207	0.487	-	-	34.963	2.058
	NUCE	7.653	4.505	0.623	4.640	11.466	21.879	2.384
	BPDHE	7.045	0.417	0.507	79.545	**29.125**	32.487	2.262
	HE	5.658	**5.076**	0.683	6.361	10.096	27.975	3.016
	AMSR	6.218	4.210	5.930	1.443	6.539	27.487	**1.825**
	LIME	7.201	1.189	0.585	285.697	23.572	26.881	2.063
	ICCV	6.952	3.072	**33.072**	**1.433**	6.568	31.130	2.184
	RCLAHE	6.854	2.977	0.541	891.186	18.631	**20.962**	2.716
	CCPF	**7.805**	5.067	2.064	1.437	6.555	32.903	3.278

Table 3 shows the average dataset for 200 sample underwater images.

Table 3. Average dataset of 200 sample underwater images.

Methods	Quantitative analysis						
	Entropy ↑	UIQM ↑	UCIQE ↑	MSE ↓	PSNR ↑	PIQE ↓	NIQE ↓
Input	7.016	2.086	0.469	0	0	29.375	3.647
NUCE	7.710	4.561	0.624	100.592	13.619	27.558	4.015
BPDHE	7.374	2.366	0.531	288.397	**21.942**	29.375	3.584
HE	5.851	4.651	0.644	4.616	11.878	28.976	3.997
AMSR	6.592	4.777	11.129	48.445	7.160	25.137	**3.583**
LIME	7.272	2.472	3.631	120.312	18.208	23.942	3.747
ICCV	7.006	4.220	**14.236**	**4.371**	7.188	25.718	3.743
RCLAHE	7.145	3.870	0.520	535.638	19.130	**21.376**	3.842
CCPF	**7.823**	**6.287**	12.579	5.176	7.215	37.558	4.946
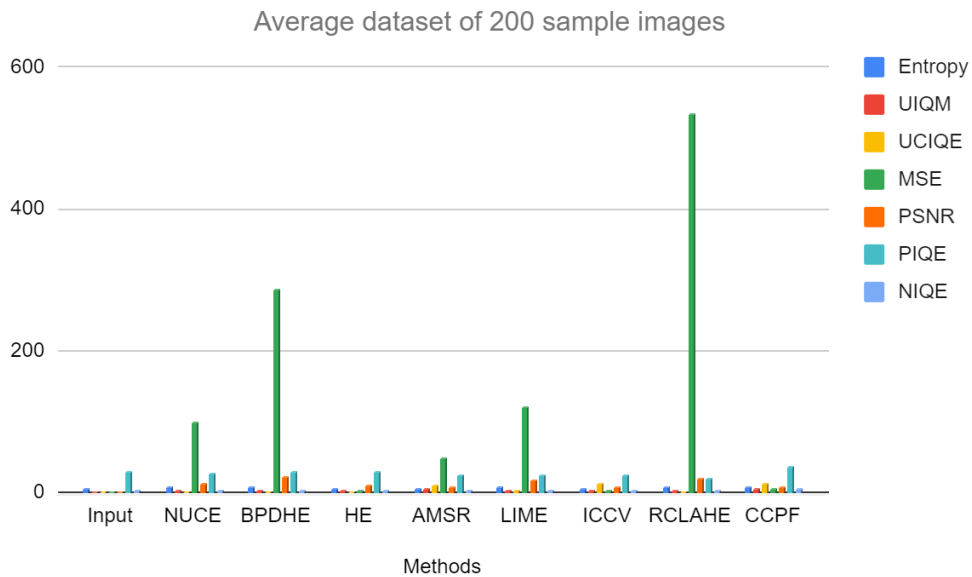
Figure 13. Visualisation of average dataset for quantitative evaluation

CONCLUSION

In this work, we suggest an improvement strategy that combines color correction with particle swarm intelligence fusion (CCPF). The following are the contributions of this work: (1) Improving the existing method's inconsistent of red channel, (2) Increase the image's brightness even further. (3) Improving the visual quality and detail image. (4) Improve image contrast. Through quantitative analysis, this method produces better results for entropy and UIQM than the prior method, with an average entropy value of 7.823 and an average UIQM value of 6.287. In future work, the study will concentrate on optimising the colour compensation technique under various colour deviations in addition to further modifying the algorithm's structure to reduce execution time. Computer vision analysis will play an increasingly significant part in the process of image processing in marine research, underwater safety, and underwater archaeology due to the widespread usage of underwater vision in a variety of scientific study domains.

ACKNOWLEDGEMENT

REFERENCES

[1]   Kewei C., Yang, Z., Pang, H., Miao, X., He, J., Liu, Y., Zhang, T., and Wang, W. (2022). A novel underwater color correction method based on underwater imaging model and generative Adversarial Network. Computers and Electronics in Agriculture, vol. 200, 107186. doi: https://doi.org/10.1016/j.compag.2022.107186

[2]   Manigandan, M., and Dhandapani, V. (2022). Underwater image enhancement by color correction and color constancy via RETINEX for detail preserving. Computers and Electrical Engineering, vol.100, 107909, doi: https://doi.org/10.1016/j.compeleceng.2022.107909

[3]   Zhang, Weidong, Dong, L., and Xu, W. (2022). Retinex-inspired color correction and detail preserved fusion for underwater image enhancement. Computers and Electronics in Agriculture, vol. 192, 106585, doi: https://doi.org/10.1016/j.compag.2021.106585

[4]   Huang, Jiayan., Xu, H., Liu, G., Wang, C., Hu, Z., and Li, Z. (2022). SIDNet: A single image dedusting network with color cast correction. Signal Processing, vol. 199, 108612, doi: https://doi.org/10.1016/j.sigpro.2022.108612

[5]   McGlamery, B. L. (1980). SPIE Proceedings, doi: https://doi.org/10.1117/12.958279

[6]   Ke K., Zhang C., Tang Q., He Y., and Yao B. (2022). Single Underwater Image Restoration based on descattering and color correction. Optik, vol. 259, 169009, doi: https://doi.org/10.1016/j.ijleo.2022.169009

[7]   Zhang, Weidong, Pan, X., Xie, X., Li, L., Wang, Z., and Han, C. (2021a). Color correction and adaptive contrast enhancement for underwater image enhancement. Computers & Electrical Engineering, vol. 91, 106981, doi:https://doi.org/10.1016/j.compeleceng.2021.106981

[8]   Zhang, Weidong, Dong, L., Zhang, T., and Xu, W. (2021b). Enhancing underwater image via color correction and bi-interval contrast enhancement. Signal Processing: Image Communication, vol. 90, 116030, doi: https://doi.org/10.1016/j.image.2020.116030

[9]   Liang, Z., Wang, Y., Ding, X., Mi, Z., and Fu, X. (2021). Single underwater image enhancement by attenuation map guided color correction and detail preserved dehazing. Neurocomputing, vol. 425, pp. 160–172, doi:https://doi.org/10.1016/j.neucom.2020.03.091

[10]   Wang, Fei, Wang, W., and Qiu, Z. (2018). Color correction algorithm for color constancy finite dimensional linear model under complex illumination. Pattern Recognition Letters, vol. 116, pp. 233–237, doi: https://doi.org/10.1016/j.patrec.2018.10.017

[11]   Mohd Azmi KZ, Abdul Ghani AS, Zulkifli Md Yusof, Ibrahim Z. (2019). Deep underwater image enhancement through colour cast removal and optimization algorithm. The Imaging Science Journal. Vol. 67, Issue 6, Pp. 330-342. DOI: https://doi.org/10.1080/13682199.2019.1660484

[12]   Abdul Ghani AS, Ab Nasir AF, Zakaria MA, Ibrahim AN. (2018). Modification of Lab color model for minimizing blue-green illumination of underwater vision system. 2018 25th IEEE International Conference on Mechatronics and Machine Vision in Practice (M2VIP). Pp. 1-7. 20-22 Nov 2019. DOI: 10.1109/M2VIP.2018.8600832

[13]   Dutta, Manoj K., Kaur, M., and Sarkar, R. K. (2022). Comparative performance analysis of Fuzzy Logic and particle swarm optimization (PSO) techniques for Image Quality Improvement: With special emphasis to old and distorted folk paintings. Optik, vol. 254, 168644, doi: https://doi.org/10.1016/j.ijleo.2022.168644

[14]   Lin, Yu-Hsien., Wang, S.-M., Huang, L.-C., and Fang, M.-C. (2017). Applying the STEREO-vision detection technique to the development of underwater inspection task with PSO-based dynamic routing algorithm for Autonomous Underwater Vehicles. Ocean Engineering, vol. 139, pp. 127–139, doi: https://doi.org/10.1016/j.oceaneng.2017.04.051

[15]   Swarup Ghosh, K., Biswas, B., and Ghosh, A. (2020). A novel approach of retinal image enhancement using PSO system and measure of fuzziness. Procedia Computer Science, vol. 167, pp. 1300–1311, doi: https://doi.org/10.1016/j.procs.2020.03.446

[16]   Shanmugavadivu, P., and Balasubramanian, K. (2014). Particle swarm optimized multi-objective histogram equalization for image enhancement. Optics & Laser Technology, vol. 57, pp. 243–251, doi: https://doi.org/10.1016/j.optlastec.2013.07.013

[17]   Acharya Upendra K. and Kumar Sandeep. (2020). Particle swarm optimized texture-based histogram equalization (PSOTHE) for MRI Brain Image Enhancement. Optik, vol. 224, 165760, doi: https://doi.org/10.1016/j.ijleo.2020.165760

[18]   Yaqiao Zhao, Yu X., Wu H., Zhou Y., Sun X., Yu S., Yu S., and Liu H. (2021). A fast 2-D otsu lung tissue image segmentation algorithm based on improved PSO. Microprocessors and Microsystems, vol. 80, 103527, doi:https://doi.org/10.1016/j.micpro.2020.103527

[19]   Kwok, N. M., Shi, H. Y., Ha, Q. P., Fang, G., Chen, S. Y., and Jia, X. (2013). Simultaneous image color correction and enhancement using particle swarm optimization. Engineering Applications of Artificial Intelligence, vol. 26(10), pp. 2356–2371, doi: https://doi.org/10.1016/j.engappai.2013.07.023

[20]   Wan Minjie., Gu G., Qian W., Ren K., Chen Q., and Maldague X. (2018). Particle swarm optimization-based local entropy weighted histogram equalization for Infrared Image Enhancement. Infrared Physics & Technology, vol. 91, pp. 164–181, doi: https://doi.org/10.1016/j.infrared.2018.04.003

[21]   Kamarul Baharin MAS, Abdul Ghani AS, Mohammad-Noor N, Ismail HN, Syamsul Amri SQ. (2022). Automatic phytoplankton image smoothing through integrated dual image histogram specification and enhanced background removal method. The Imaging Science Journal. Pp. 1-27. DOI: https://doi.org/10.1080/13682199.2022.2149067

[22]   Yuan, J., Cai, Z., and Cao, W. (2022). TEBCF: Real-world underwater image texture enhancement model based on blurriness and color fusion. IEEE Transactions on Geoscience and Remote Sensing, vol. 60, pp. 1–15, doi:https://doi.org/10.1109/tgrs.2021.3110575

[23]   Kennedy, J., and Eberhart R., (1995). "Particle swarm optimization". *International Conference on Neural Networks*, vol. 4, pp 1942-1948, doi:10.1109/ICNN.1995.488968

[24]   Mohd Azmi, K. Z., Abdul Ghani, A. S., Md Yusof, Z., and Ibrahim, Z. (2019). Natural-based underwater image color enhancement through fusion of swarm-intelligence algorithm. Applied Soft Computing, vol. 85, 105810, doi:https://doi.org/10.1016/j.asoc.2019.105810

[25]   Ibrahim, H., and Pik Kong, N. (2007). Brightness preserving dynamic histogram equalization for image contrast enhancement. IEEE Transactions on Consumer Electronics, vol. 53(4), pp. 1752–1758, doi: https://doi.org/10.1109/tce.2007.4429280

[26]   Yu Wang, Qian Chen, and Baeomin Zhang. (1999). Image enhancement based on equal area dualistic sub-image histogram equalization method. IEEE Transactions on Consumer Electronics, vol. 45(1), pp. 68–75, doi: https://doi.org/10.1109/30.754419

[27]   Lee, C.-H., Shih, J.-L., Lien, C.-C., and Han, C.-C. (2013). Adaptive multiscale retinex for image contrast enhancement. 2013 International Conference on Signal-Image Technology & Internet-Based Systems, doi: https://doi.org/10.1109/sitis.2013.19

[28]   Guo, X., Li, Y., and Ling, H. (2017). Lime: Low-light image enhancement via Illumination Map Estimation. IEEE Transactions on Image Processing, vol. 26(2), pp. 982–993, doi: https://doi.org/10.1109/tip.2016.2639450

[29]   Ying, Z., Li, G., Ren, Y., Wang, R., and Wang, W. (2017). A new low-light image enhancement algorithm using camera response model. 2017 IEEE International Conference on Computer Vision Workshops (ICCVW), doi:https://doi.org/10.1109/iccvw.2017.356

[30]   Abdul Ghani, A. S., and Mat Isa, N. A. (2015). Enhancement of low-quality underwater image through integrated global and local contrast correction. Applied Soft Computing, vol. 37, pp. 332–344, doi: https://doi.org/10.1016/j.asoc.2015.08.033

[31]   Jin Wu, Honglin Huang, Ya Qiu, Huaiyu Wu, Jinwen Tian, & Jian Liu. (2005). Remote sensing image fusion based on average gradient of wavelet transform. IEEE International Conference Mechatronics and Automation, doi:https://doi.org/10.1109/icma.2005.1626836

[32]   Panetta, K., Gao, C., and Agaian, S. (2016). Human-visual-system-inspired underwater image quality measures. IEEE Journal of Oceanic Engineering, vol. 41(3), pp. 541–551, doi: https://doi.org/10.1109/joe.2015.2469915

[33]   Yang, M., and Sowmya, A. (2015). An underwater color image quality evaluation metric. IEEE Transactions on Image Processing, vol. 24(12), pp. 6062–6071, doi:https://doi.org/10.1109/tip.2015.2491020

[34]   Z. Wang and A. C. Bovik, (2009), "Mean Squared Error: Love It or Leave It? A New Look at Signal Fidelity Measures." IEEE Signal Processing Magazine, vol. 26, no. 1, pp. 98–117., doi: https://doi.org/10.1109/msp.2008.930649

[35]   Hore, A., and Ziou, D. (2010). Image quality metrics: PSNR vs. SSIM. 2010 20th International Conference on Pattern Recognition, doi:https://doi.org/10.1109/icpr.2010.579

[36]   Venkatanath N, Praneeth D, Maruthi Chandrasekhar Bh, Channappayya, S. S., and Medasani, S. S. (2015). Blind image quality evaluation using perception-based features. 2015 Twenty First National Conference on Communications (NCC), doi:https://doi.org/10.1109/ncc.2015.7084843

[37]   Mittal, A., Soundararajan, R., and Bovik, A. C. (2013). Making a "completely blind" Image quality analyzer. IEEE Signal Processing Letters, vol. 20(3), pp. 209–212, doi:https://doi.org/10.1109/lsp.2012.2227726